Electronic Supplementary Material (ESI) for Catalysis Science & Technology.
This journal is © The Royal Society of Chemistry 2017

Supplementary Information for

Electrocatalytic Hydrogenation of Pyridinium Enabled by Surface Proton Transfer Reactions

Coleman X. Kronawitter,[ar] Zhu Chen,[a] Peng Zhao,[b] Xiaofang Yang,[a] Bruce E. Koel[a]

[a]Department of Chemical and Biological Engineering, Princeton University, Princeton, NJ 08544 (USA)

[b]Department of Chemistry, Princeton University, Princeton, NJ 08544 (USA)

[r]Current address: Department of Chemical Engineering, University of California, Davis, Davis, CA 95616 (USA)

*Email: bkoel@princeton.edu. Tel.: 609-258-4524.

I. Experimental details

Operando FTIR absorption spectra were obtained with a Bruker Vertex 70 FTIR with a specular reflectance accessory (Veemax III, Pike Technologies). An electrochemical cell enabled reflectance measurements from the surface of a polycrystalline Pt electrode under applied potential. An Ag/AgCl reference electrode and a Pt wire counter electrode were used. In this setup the incident IR beam passes through a CaF_2 window and a thin layer of electrolyte before and after reflecting from the electrode surface. Reference FTIR absorption spectra for pyridine and piperidine were obtained using attenuated total reflection (Harrick Horizon Multiple Reflection). In this case, neat pyridine and piperidine and solutions of 50 vol% pyridine in 0.5 M H_2SO_4 and 50 vol% piperidine in 0.5 M H_2SO_4 were pipetted directly onto a ZnSe ATR element. For all FTIR measurements, the resolution was 4 cm^{-1}. For adsorption experiments, a polycrystalline Pt wire was used as the working electrode, and the current density was reported with respect to the electrochemically active surface area, defined by 1 monolayer hydrogen deposition in the underpotential regime. Chemicals: pyridine (Aldrich, >99.9%); benzene (Aldrich, >99.9%); piperidine (Aldrich, >99.5%); pyridine-d_5 (Aldrich, 99.5 atom% D); D_2O (Cambridge Isotope Laboratories, Inc., 99.9%).

II. *Operando* FTIR probing pyridinium hydrogenation during CVs

Fig. 1c in the main text shows CVs in the absence and presence of pyridinium. Fig. S1 below shows FTIR spectra acquired during 288 s of CV cycling under the conditions associated with Fig. 1c, between 0.2 and -0.45 $V_{Ag/AgCl}$. The intensities of the features associated with the hydrogenation of pyridinium increase with time and then stabilize.

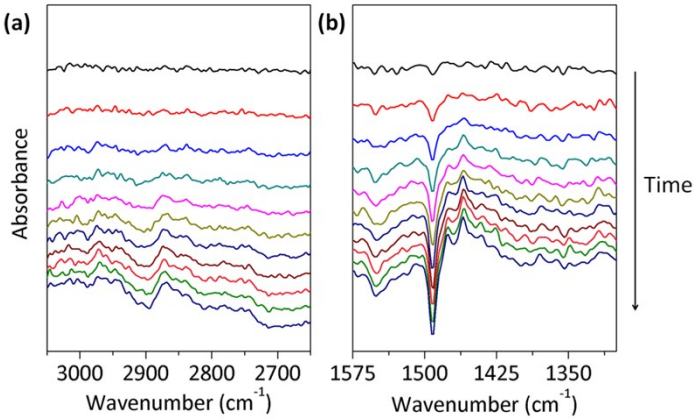

Figure S1. *Operando* FTIR spectra characterizing the near-surface region of Pt in 0.1 M pyridinium during CV scanning in Fig. 1c of the main text. (a) Magnification of the energy range associated with CH_2 stretching modes. (b) Magnification of energy range associated with ring and CH_2 bending modes. Each spectrum was signal-averaged for 32 s.

III. Pyridine-d_5 deuteration/hydrogenation

The electrocatalytic hydrogenation of pyridinium was studied with deuterium isotope labeling. This permitted evaluation of spectral ranges that are dominated by H_2O vibrational bands in H_2O-based electrolytes and confirmed CH_2 stretching band assignments. Pyridine-d_5 was dissolved in D_2O with 0.5 M H_2SO_4, and *operando* reflectance FTIR spectra were recorded during CA at various potentials. Fig. S2 shows representative data collected during CA at -0.35 $V_{Ag/AgCl}$. As expected, the CD_2 stretch modes are now observed near 2200 cm^{-1}. The five negative peaks in the energy range corresponding to ring modes and CH_2 bending modes (1600 to 1250 cm^{-1}) result from the consumption of pyridinium possessing both D and H, with H resulting from D-H exchange and/or H hydrogenation associated with the use of H_2SO_4 and perhaps H_2O contamination from air exposure.

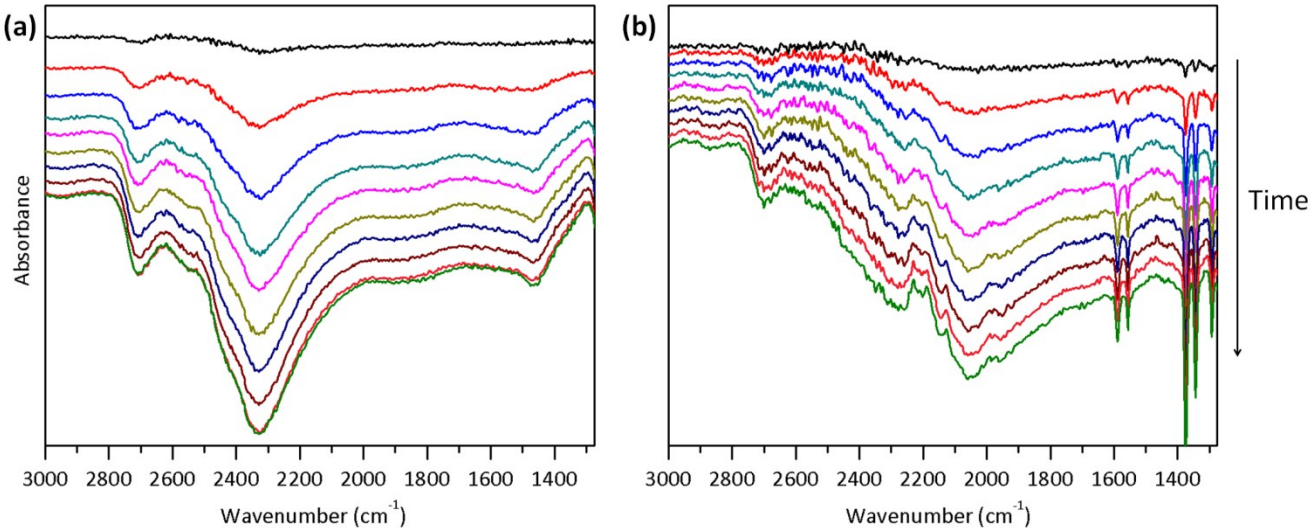

Figure S2. *Operando* reflectance FTIR spectra characterizing the near-surface region of Pt during CA at -0.35 $V_{Ag/AgCl}$ in D_2O and 0.5 M H_2SO_4 (a) without and (b) with 0.1 M pyridine-d_5. Each spectrum was signal-averaged for 32 s. CD_2 stretching bands near 2200 cm^{-1} are noted.

IV. *Operando* reflectance FTIR probing pyridinium hydrogenation in the presence of CO_2

Electrocatalytic hydrogenation of pyridinium was studied under the same conditions as those associated with Fig. 1 of the main text, but in the presence of dissolved CO_2 (Fig. S3-4). No notable differences were observed due to the presence of CO_2, with the exception of the new peak at 2350 cm^{-1}, which corresponds to dissolved CO_2. The high-energy shoulder on this peak is attributed to gas-phase CO_2, resulting from the nucleation of CO_2 bubbles at the CaF_2 window.

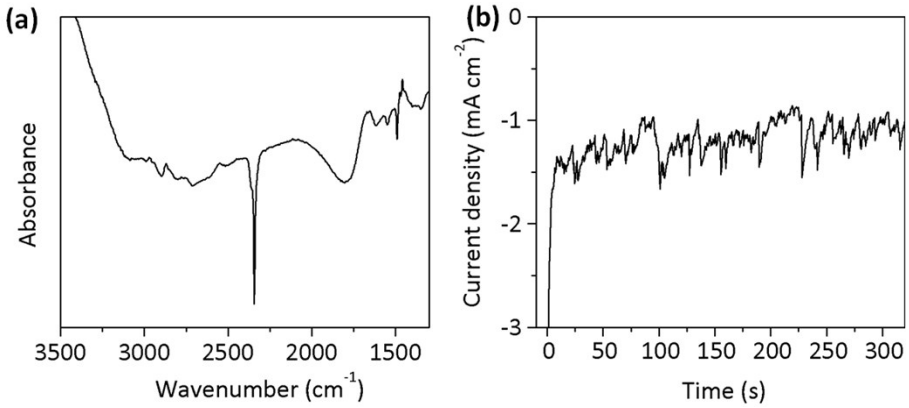

Figure S3. *Operando* FTIR spectra characterizing the near-surface region of Pt in 0.5 M H_2SO_4, 0.1 M pyridinium, saturated with CO_2. (a) FTIR spectrum, signal-averaged during 320 s of CA at -0.45 $V_{Ag/AgCl}$. (b) CA trace recorded during the FTIR measurement in (a).

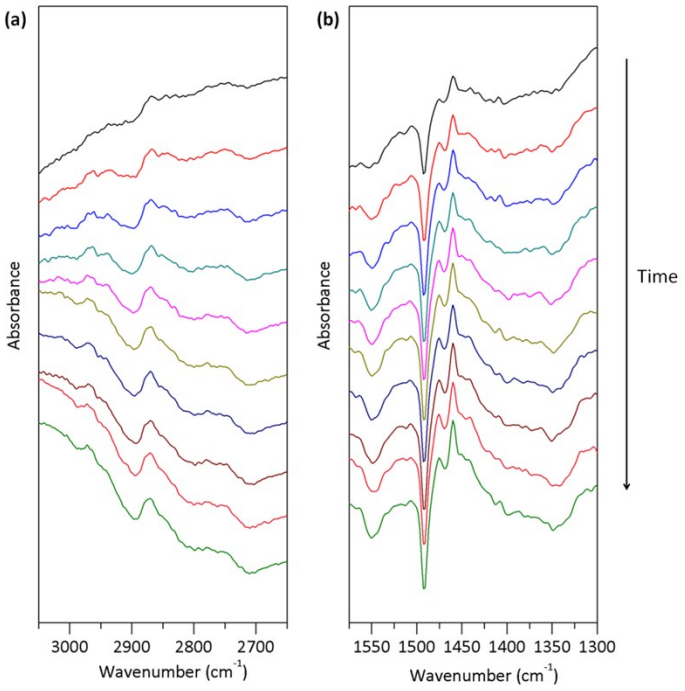

Figure S4. *Operando* reflectance FTIR spectra characterizing the near-surface region of Pt in 0.5 M H_2SO_4, 0.1 M pyridinium, saturated with CO_2, during CA for 320 s at -0.45 $V_{Ag/AgCl}$. Each spectrum is signal-averaged for 32 s. (a) Energy range associated with CH_2 stretching modes. (b) Energy range associated with ring and CH_2 bending modes.

V. Discussion of the *operando* reflectance FTIR thin-layer electrochemical cell

We performed experiments to characterize the thin-layer electrochemical cell used for our FTIR measurements. We studied the scan rate dependence of hydrogen adsorption and desorption in the underpotential regime (Fig. S5). Underpotential adsorption and desorption of hydrogen on Pt shows reversible kinetics when Pt is displaced from the FTIR sampling position, which is well-known for this process in the literature. However, when Pt is placed in the FTIR sampling position and mass transport is constrained by the thin-layer geometry, hydrogen adsorption/desorption shows quasi-reversible characteristics. In the FTIR position, the cathodic apex potential was limited to -0.3 $V_{Ag/AgCl}$ so that H_2 bubbles did not displace H_2O (see below) and interfere with the scan rate trend.

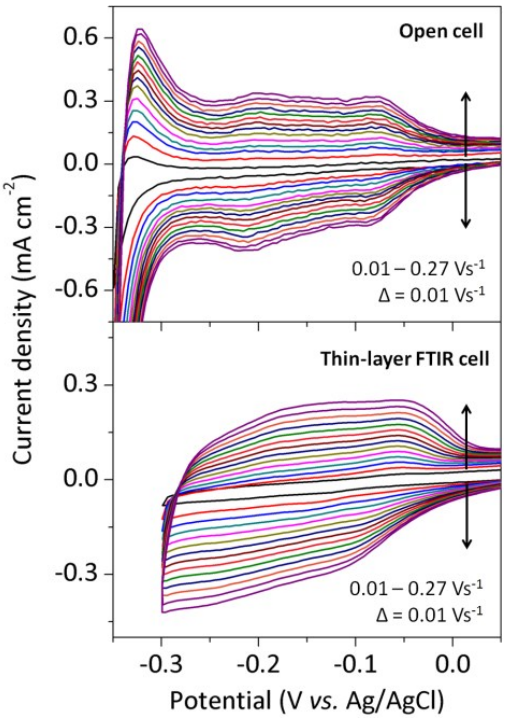

Figure S5. CVs showing the hydrogen adsorption/desorption regime for Pt in 0.5 M H_2SO_4 at fourteen different scan rates at 0.01 Vs^{-1} increments, with Pt away from the FTIR acquisition position (top) and in the FTIR acquisition position (bottom). The results demonstrate quasi-reversible proton reduction when the Pt surface is in the FTIR sampling position.

To further characterize the system, and specifically to examine the effects of displaced H_2O, FTIR spectra were recorded for a variety of electrochemical conditions. Fig. S6 shows spectra recorded during CV cycles between 0.2 and -0.27 $V_{Ag/AgCl}$ in 0.5 M H_2SO_4 (Fig. S6a) and 0.5 M H_2SO_4 containing 0.1 M pyridinium (Fig. S6b). The small negative peaks near 2350 cm^{-1} are due to an experimental artifact resulting from slight fluctuations of CO_2 levels inside the N_2-purged optics boxes in the beam path outside of the electrochemical cell.

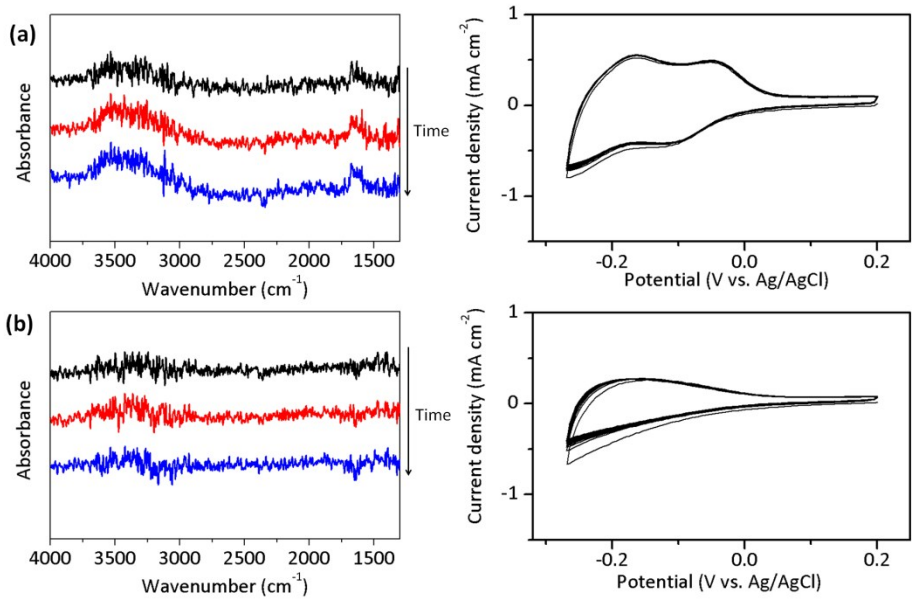

Figure S6. *Operando* FTIR spectra characterizing the near-surface region of Pt during CV cycles between 0.2 and -0.27 $V_{Ag/AgCl}$ in (a) 0.5 M H_2SO_4 and (b) 0.5 M H_2SO_4 containing 0.1 M pyridinium. Each FTIR spectrum was signal-averaged for 64 s. CV curves corresponding to the spectra are adjacent to the right; 0.2 Vs^{-1}.

When H_2 evolution occurs, the IR absorbance corresponding to liquid water decreases, suggesting the displacement of H_2O from the thin layer volume that is probed by the infrared beam. The spectroscopic features of liquid H_2O are very broad due to extensive H-bonding effects. This claim was confirmed by monitoring the absorbance during H_2 evolution. Fig. S7 shows typical results, in this case obtained during CV cycles between 0.2 and -0.75 $V_{Ag/AgCl}$. Similar results were obtained at other potentials.

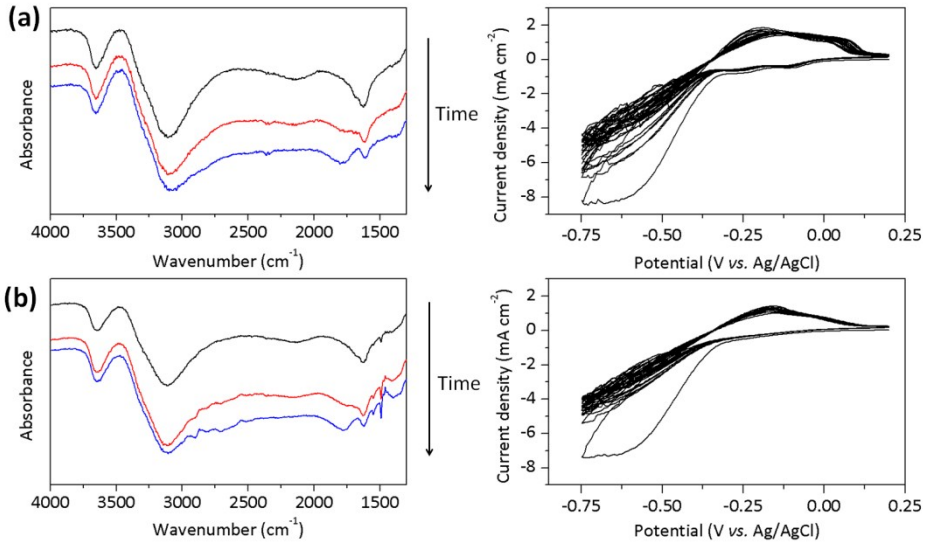

Figure S7. *Operando* FTIR spectra characterizing the near-surface region of Pt during CV cycles between 0.2 and -0.75 $V_{Ag/AgCl}$ in (a) 0.5 M H_2SO_4 and (b) 0.5 M H_2SO_4 containing 0.1 M pyridinium. Each spectrum was signal-averaged for 64 s. CV data corresponding to the spectra are adjacent to the right; 0.2 Vs^{-1}.

Oxidation of benzene was also studied. Fig. S8 shows *operando* FTIR spectra during CA at 0.7 $V_{Ag/AgCl}$ in the presence of 0.1 M benzene. As expected, the oxidation of benzene yields dissolved CO_2 as a product. Because CO_2 cannot adsorb on Pt in these conditions, this measurement provides evidence that the majority of the IR signal is from the thin layer of solution.

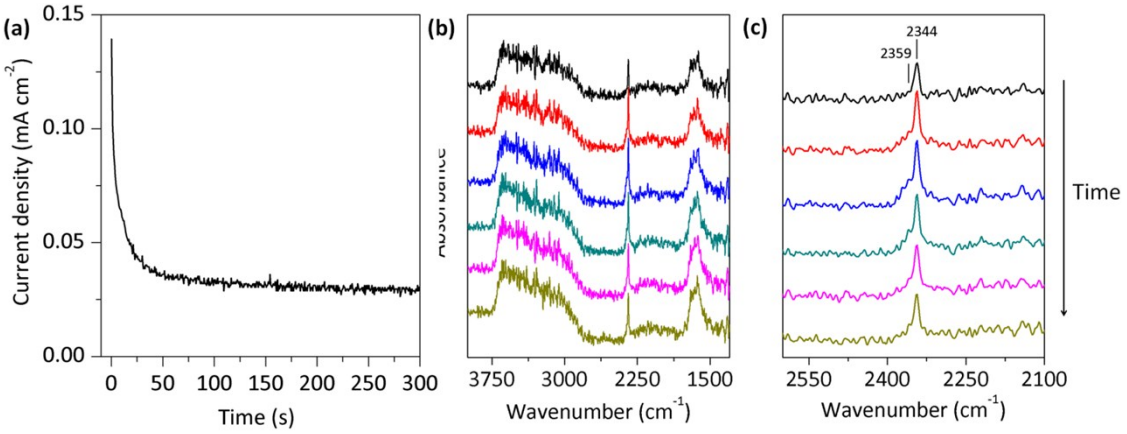

Figure S8. *Operando* FTIR spectra characterizing the near-surface region of Pt during benzene oxidation. (a) CA recorded while holding the potential at 0.7 $V_{Ag/AgCl}$ in 0.5 M H_2SO_4 containing 0.1 M benzene. (b) Broad spectral range for the FTIR curves. (b) Magnification of energy range in FTIR associated with CO_2 stretching modes. Each FTIR spectrum was signal-averaged for 96 s.

Supporting Information References

(1) Limbach, H. H.; Hennig, J.; Stulz, J. *J. Chem. Phys.* 1983, **78**, 5432.